Numerical Heat Transfer, Part A: Applications: An International Journal of Computation and Methodology
Publication details, including instructions for authors and subscription information:
http://www.tandfonline.com/loi/unht20

NUMERICAL ANALYSIS OF A BURNING DROPLET WITH INTERNAL CIRCULATION IN A GRAVITATIONAL ENVIRONMENT

Lung-Weei Huang [a] & Chiun-Hsun Chen [a]
[a] Department of Mechanical Engineering , National Chiao Tung University , Hsinchu, Taiwan, 30050, Republic of China
Published online: 15 Mar 2007.

To cite this article: Lung-Weei Huang & Chiun-Hsun Chen (1998) NUMERICAL ANALYSIS OF A BURNING DROPLET WITH INTERNAL CIRCULATION IN A GRAVITATIONAL ENVIRONMENT, Numerical Heat Transfer, Part A: Applications: An International Journal of Computation and Methodology, 34:1, 43-60, DOI: 10.1080/10407789808913976

To link to this article: http://dx.doi.org/10.1080/10407789808913976

NUMERICAL ANALYSIS OF A BURNING DROPLET WITH INTERNAL CIRCULATION IN A GRAVITATIONAL ENVIRONMENT

Lung-Weei Huang and Chiun-Hsun Chen
Department of Mechanical Engineering, National Chiao Tung University, Hsinchu, Taiwan 30050, Republic of China

A theoretical analysis of steady burning droplets with internal circulation in the presence of normal atmosphere and gravity is presented. The normalized system governing the gas phase consists of the complete set of conservation equations in r-z coordinates and includes finite-rate global kinetics. For the liquid phase, it includes continuity and momentum conservation equations. Thermodynamic equilibrium is assumed along the gas-liquid interface, which is not stationary. A body-fitted grid generation technique is used to handle irregular boundaries. The parametric study is performed by changing droplet diameter. The induced convection flow field is presented to demonstrate its interaction with the flame and the liquid flow motion. The predicted results show that there exists one, two, or three cells within the burning droplet, depending on its diameter. The occurrence of an extra cell is due to reverse flow in the gas phase generated by interaction of the induced flow and blowing velocity. Comparison with the case where internal flow is not considered, for a small droplet the effect of internal circulation on mass evaporation rate can be neglected. On the other hand, the internal flow will increase the mass evaporation rate.

INTRODUCTION

The present work is concerned with the steady burning behavior of a liquid fuel droplet with an internal circulation in an atmospheric environment. Since the droplet is so small, it is very difficult to observe the internal circulation directly by experimental means, and a simulation model becomes an important tool when attacking such problems. However, most simulation works in the past assumed that the droplet behaves as a porous solid sphere and/or burns in a convection-free field; see the review papers by Williams [1], Faeth [2], and Law [3], for example. In practice, as the schematic configuration in Figure 1 shows, a naturally convective flow will be present in the neighborhood of the droplet due to combustion, in addition to the blowing velocity from the evaporating surface. Many laboratory experiments [4–6] confirmed that free convection significantly changes the combustion characteristics of liquid droplets. For example, the flame is no longer spherical in shape, but oval. The shear stress, resulting from these two flow motions, along

Received 3 July 1997; accepted 3 March 1998.

Financial support of this research by the National Science Council of the Republic of China under Project NSC 83-0401-E-009-003 is greatly appreciated.

Address correspondence to Professor Chiun-Hsun Chen, Department of Mechanical Engineering, National Chiao Tung University, 1001 Ta Hsueh Road, Hsinchu, Taiwan 30050, Republic of China.

Numerical Heat Transfer, Part A, 34:43–60, 1998

1040–7782/98 $12.00 + .00

NOMENCLATURE

$\bar{C}_p$	average specific heat	v	nondimensional velocity in r direction
$\bar{d}$	droplet diameter	Y_f	mass fraction of fuel ($= \bar{\rho}_f/\bar{\rho}$)
$\bar{D}$	dimensional species diffusivity	Y_o	mass fraction of oxidizer $[= (\bar{\rho}_o/\bar{\rho})/Y_{o_\infty}]$
Da	Damköhler number		
E	nondimensional activation energy for gas phase reaction ($= \bar{E}/R^o\bar{T}^*$)	$\bar{z}$	distance along z direction
		$\bar{\mu}^*$	reference dynamic viscosity
f	stoichiometric oxidizer/fuel mass ratio	$\bar{\nu}$	kinematic viscosity
Gr	Grashof number	$\bar{\rho}^*$	reference fluid density
	$(= \bar{g}(\bar{\rho}_\infty - \bar{\rho})\bar{d}^3/\bar{\rho}^*\bar{\nu}^{*2})$	φ	equivalence ratio
Gr_l	liquid Grashof number $[= Gr(\rho_l\bar{\mu}^*/\bar{\rho}^*\mu_l)^2]$	$\bar{\omega}$	reaction rate
$\bar{k}$	thermal conductivity		
L	nondimensional latent heat of fuel ($= \bar{L}/\bar{C}_p\bar{T}^*$)	**Subscripts**	
Le	Lewis number ($= \bar{\alpha}/\bar{D}$)	f	fuel
p	nondimensional pressure	l	liquid phase
Pr	Prandtl number ($= \bar{C}_p\bar{\mu}/\bar{k}$)	n, t	normal and tangential to droplet surface
Q	nondimensional heat of combustion ($= \bar{Q}/\bar{C}_p\bar{T}^*$)	o	oxidizer
		w	surface of the droplet
$\bar{r}$	distance in r direction	∞	ambient
R^o	universal gas constant		
T	nondimensional temperature	**Superscripts**	
u	nondimensional velocity in z direction		
U_{ref}	reference velocity $\{= [\bar{g}(\bar{\rho}_\infty - \bar{\rho}_f)\bar{d}/\bar{\rho}^*]^{1/2}\}$	*	reference state
		-	dimensional quantities

the droplet surface leads the liquid fuel to flow internally. This internal flow brings heat from the surface to the inside of the droplet which affects the evaporation rate and fluid motion at the interface. It further influences the flow field and thermal field in the gas phase and, eventually, the heat transfer rate along the fuel surface. These physical processes indicate that the gas and liquid phases are coupled together and should be considered at the same time. Apparently, the interaction makes the problem extremely complex, and an analytical solution is almost impossible.

Batchelor [7] analyzed isothermal internal droplet motion by assuming a thin viscous boundary layer exists near the droplet surface at large Reynolds numbers, Re. The results indicated that the motion in the droplet core is still a Hill's vortex. Later, Rivkind et al. [8] numerically solved the Navier-Stokes equations in both the liquid and gas phases. They found that the internal streamline patterns are similar to those of Hill's vortex for a wide range of Re. For droplet vaporization at intermediate-Re flow, Prakash and Sirignano [9, 10] developed a theoretical model to study the influence of internal circulation on droplet evaporation rate. They employed a boundary layer analysis and an assumption of quasi-steadiness in both gas and liquid phases. By assuming an approximate shear stress distribution at the

droplet surface [9], they investigated the effect of internal circulation on droplet temperature for two different boundary conditions: a given temperature gradient and a specified temperature at the droplet surface. Later, they extended this liquid phase model to solve the coupled gas phase equations [10]. The results showed that liquid heating persists through almost the entire droplet lifetime, indicating that the droplet vaporation process is unsteady and the droplet temperature is nonuniform. However, the boundary layer assumption was not very compatible with the Re range (Re $\approx$ 100) and was completely invalid beyond the separation point. From the work of Huang and Ayyaswamy [11], they pointed out that a boundary layer analysis is not enough to describe the evaporation process during the entire droplet lifetime. They also mentioned that assumptions of constant surface temperature and constant properties will likely lead to errors in the estimations of heat and mass transfer to an evaporating drop.

Following the work of Prakash and Sirignano [10], many investigators began to use the complete Navier-Stokes equations. By solving the complete set of governing equations, in which the gas and liquid phases were coupled together, Chiang et al. [12] and Renksizbulut et al. [13, 14] numerically studied droplet vaporization at intermediate-Re flow in a high-temperature environment. Included in these studies were initial droplet temperature, ambient temperature, initial Re, droplet heating model, variable thermophysical properties, liquid phase motion and heating, and transient variation in the droplet size and velocity. The results showed that the liquid phase motion is a slow transient that decreases with a decrease in the free-stream Re (or a decrease in droplet diameter), and the liquid motion must be considered unsteady. In addition, droplet heating is also a major factor in droplet unsteadiness behavior. Some correlations with drag coefficient, Nusselt, and Sherwood numbers were also given in these studies.

Lin [15] performed an experimental study to investigate droplet heating mechanisms under a convective flow environment. By measuring transient internal droplet temperature distribution, the effects of Re (17, 60, or 100) and liquid viscosity on internal droplet dynamics and heating mechanisms were investigated. The results showed that the droplet center temperature is higher than the two symmetrically located off-center temperatures during droplet heating. Also the internal vortex motion indeed enhances internal heat transport. In addition, the vortex model developed by Prakash and Sirignano [9, 10] might be quantitatively overpredictive in determining the internal temperature distribution of a droplet because they overestimated the internal liquid velocity. The radial temperature distribution measurements showed the temperature distribution along a streamline is far from isothermal, unlike the isothermal streamlines used in the vortex model. Increasing liquid viscosity results in a decrease in the internal circulation and, consequently, the heat transport rate.

Ayyaswamy et al. [16] investigated the effect of internal circulation on the transport in a moving drop at low-Re flow (Re $<$ 1). Their results showed that an increase in radial evaporation velocity will lead to a decrease in the strength of internal circulation, and for a sufficiently large evaporation velocity, the internal circulation may vanish or even reverse. Since the maximum evaporation velocity is at the front stagnation point, the shear stress generated by the variation of

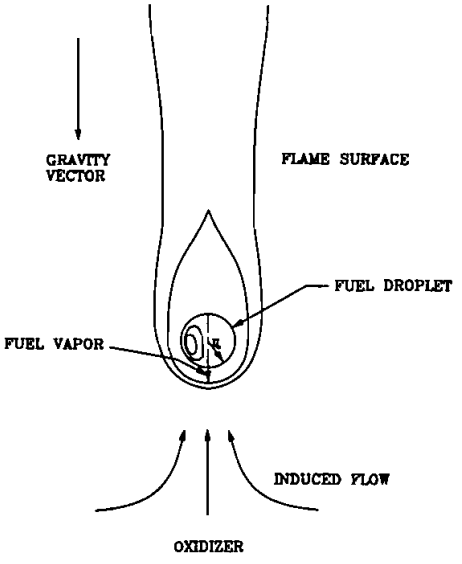

Figure 1. Flow field configuration.

nonuniform radial evaporation velocity in the angular direction opposes the usual circulation. Obviously, the radial evaporation velocity also plays an important role in liquid phase motion at low-Re flows. Later, Jog et al. [17] analyzed the evaporation and combustion of an n-heptane fuel droplet, moving slowly (Re = 0.2) in a hot oxidant atmosphere, by using perturbation methods. The gas and liquid phase results, such as flow fields, temperature and species distributions, as well as heat and mass transfer along the interface were all correct to second order. They found that in comparison with the first-order theory, the second-order theory obtains that both the flame and the front stagnation point are closer to the droplet surface, the evaporation is more vigorous, the droplet lifetime is shorter, and the internal vortical motion is asymmetric about the drop equatorial plane.

Law [18] and Law and Sirignano [19] investigated the unsteady effects of heating on droplet combustion. They assumed that the droplet temperature is spatially uniform but varies temporally for the liquid phase [18], and the droplet temperature is governed primarily by the heat conduction equation [19]. Their results indicated that droplet heating is an important process and should be considered in an unsteady droplet combustion problem. However, this simplified model did not consider the effects of internal circulation and convective flow field. Dwywer and Sanders [20, 21] developed a combustion model, consisting of the full set of two-dimensional conservation equations with finite-rate global kinetics of the gas phase. They clearly demonstrated the effect of Re on droplet combustion, and the transition from a wake flame to an envelope flame. However, flow in the liquid phase was not considered in their model and led to a disagreement with a "liquid" droplet boundary.

Finally, Kneer et al. [22] studied the effect of variation of liquid properties on evaporation of the multicomponent droplets by using an extension of the Diffusion Limit Model. The results showed that the evaporation process is substantially

affected by the temperature and concentration dependence of the liquid properties, implying that the commonly used model of constant property needs improvement. Also, remarkable variations of the droplet refractive index are observed, indicating that the estimation of errors in optical particle sizing techniques should take this effect into consideration.

From the above review, we can see that, so far, only works dealing with the pure vaporization process of a droplet subjected to a hot forced flow (without combustion) have considered the interaction between gas and liquid phases. When burning was considered, either the droplet itself was treated as a porous solid sphere, or the flow field and thermofield in the gas phase were specified in advance. Therefore, we attempt to set up a steady combustion model to simulate and study the interaction between the internal flow of a burning droplet and its flame in normal gravity. Natural convection will be built up around the droplet as a result of the motion of fluid due to the density change arising from the flame appearance. Then, it simultaneously affects the flame itself via the flow stretching effect. However, this flow field is not known a priori but is provided as part of the solution. A parametric study is given by changing the droplet diameter. The complete flame structures and the corresponding flow within the droplet are demonstrated in detail. Also, the evaporation rates are compared with those of a previous work [23], in which the liquid flow was not considered, in order to better understand the limitation of such assumption on droplet combustion.

MATHEMATICAL FORMULATION

On the basis of the previous discussion, we can establish a combustion model accordingly. Because the emphasis in the present study is on the interaction between gas and liquid phases and not on the transient behavior, we assume the problem to be steady. Thus consideration of the gas phase requires a set of differential conservation equations for continuity, momentum, energy, and species. An equation of state, a relationship of viscosity variation with temperature, and a number of assumptions that serve to link these properties are used. A chemical reaction is used to describe the combustion process. In the liquid phase, the droplet temperature is spatially uniform due to the steady state assumption; therefore a continuity equation and momentum equations are sufficient to describe flow motion. The interface boundary conditions should be consistent with thermodynamic equilibrium, the continuity of shear stress, the tangential velocity and temperature, and the conservation of mass flux, energy, and species. Finally, a set of known boundary conditions for the gas and liquid phases are specified to complete the mathematical model.

In order to make the problem more tractable, the following assumptions are made. (1) The droplet retains a spherical shape throughout. (2) The flows are laminar and axisymmetric. (3) Radiative heat transfer and bulk viscosity effects are ignored. (4) The ideal gas law is applicable to the gas mixture with constant and equal specific heat, equal diffusion coefficients, and constant Prandtl and Lewis numbers. (5) Viscous dissipation and compressive work are ignored because of low-speed convection. (6) Gas phase combustion is described by a one-step overall chemical reaction; $1[\mathrm{F}] + f[\mathrm{O}] \rightarrow (1 + f)\ [\mathrm{P}] + \bar{q}$, where f and $\bar{q}$ represent the

stoichiometric oxidizer/fuel mass ratio and the heat of combustion per unit mass of fuel, respectively. The fuel is ethanol, and the corresponding consumption rate is adopted from Westbrook and Dryer [24]. After a mathematical manipulation, it is expressed as $\bar{\omega}_f = \bar{B}\bar{Y}_{o_\infty}^{1.6}\bar{\rho}^{1.75}Y_f^{0.15}Y_o^{1.6}\exp(-\bar{E}/R^o\bar{T})$, where $Y_o = \bar{Y}_o/\bar{Y}_{o_\infty}$.

Before the actual computation, a nondimensionalization procedure is performed. Because there is no explicit reference velocity for naturally convective flows, we follow the choice of Chen and Hou [25] in defining a reference velocity chosen by equating the buoyancy and inertia forces to obtain the following expression:

$$\bar{U}_{\text{ref}} = \left(\frac{\bar{g}(\bar{\rho}_\infty - \bar{\rho}_f)\bar{d}}{\bar{\rho}^*}\right)^{1/2} \tag{1}$$

where the asterisk represents the quantities evaluated at the arithmetic average of the adiabatic flame temperature and ambient temperature. The nondimensional procedure is not repeated here; interested readers can refer to Ref. [23] for further details.

The dimensionless governing equations are as follows.

Gas Phase

Continuity

$$\frac{\partial(\rho u)}{\partial z} + \frac{1}{r}\frac{\partial(\rho v r)}{\partial r} = 0 \tag{2}$$

z-Momentum

$$\rho u\frac{\partial u}{\partial z} + \rho v\frac{\partial u}{\partial r} = -\frac{\partial p}{\partial z} + \frac{\bar{\rho}_\infty - \bar{\rho}}{\bar{\rho}_\infty - \bar{\rho}_f} + \frac{\partial}{\partial z}\left\{\frac{\mu}{\sqrt{\text{Gr}}}\left[2\frac{\partial u}{\partial z} - \frac{2}{3}\left(\frac{1}{r}\frac{\partial}{\partial r}(rv) + \frac{\partial u}{\partial z}\right)\right]\right\} + \frac{1}{r}\frac{\partial}{\partial r}\left[\frac{\mu}{\sqrt{\text{Gr}}}r\left(\frac{\partial u}{\partial r} + \frac{\partial v}{\partial z}\right)\right] \tag{3}$$

r-Momentum

$$\rho u\frac{\partial v}{\partial z} + \rho v\frac{\partial v}{\partial r} = -\frac{\partial p}{\partial r} + \frac{1}{r}\frac{\partial}{\partial r}\left\{r\frac{\mu}{\sqrt{\text{Gr}}}\left[2\frac{\partial v}{\partial r} - \frac{2}{3}\left(\frac{1}{r}\frac{\partial}{\partial r}(rv) + \frac{\partial u}{\partial z}\right)\right]\right\} + \frac{\partial}{\partial z}\left[\frac{\mu}{\sqrt{\text{Gr}}}\left(\frac{\partial u}{\partial r} + \frac{\partial v}{\partial z}\right)\right] + \frac{\mu}{\sqrt{\text{Gr}}}\frac{1}{r}\left\{\frac{2v}{r} - \frac{2}{3}\left[\frac{1}{r}\frac{\partial}{\partial r}(rv) + \frac{\partial u}{\partial z}\right]\right\} \tag{4}$$

Energy

$$\rho u\frac{\partial T}{\partial z}+\rho v\frac{\partial T}{\partial r}=\frac{1}{\sqrt{\mathrm{Gr}}\,\mathrm{Pr}}\left[\frac{1}{r}\frac{\partial}{\partial r}\left(r\mu\frac{\partial T}{\partial r}\right)+\frac{\partial}{\partial z}\left(\mu\frac{\partial T}{\partial z}\right)\right]+Q\dot{\omega}_{\mathrm{f}} \tag{5}$$

Fuel species

$$\rho u\frac{\partial Y_{\mathrm{f}}}{\partial z}+\rho v\frac{\partial Y_{\mathrm{f}}}{\partial r}=\frac{1}{\mathrm{Le}\,\mathrm{Pr}\sqrt{\mathrm{Gr}}}\left[\frac{1}{r}\frac{\partial}{\partial r}\left(r\mu\frac{\partial Y_{\mathrm{f}}}{\partial r}\right)+\frac{\partial}{\partial z}\left(\mu\frac{\partial Y_{\mathrm{f}}}{\partial z}\right)\right]-\dot{\omega}_{\mathrm{f}} \tag{6}$$

Oxidizer species

$$\rho u\frac{\partial Y_{\mathrm{o}}}{\partial z}+\rho v\frac{\partial Y_{\mathrm{o}}}{\partial r}=\frac{1}{\mathrm{Le}\,\mathrm{Pr}\sqrt{\mathrm{Gr}}}\left[\frac{1}{r}\frac{\partial}{\partial r}\left(r\mu\frac{\partial Y_{\mathrm{o}}}{\partial r}\right)+\frac{\partial}{\partial z}\left(\mu\frac{\partial Y_{\mathrm{o}}}{\partial z}\right)\right]-\frac{f}{Y_{\mathrm{o}_\infty}}\dot{\omega}_{\mathrm{f}} \tag{7}$$

where

$$\dot{\omega}_{\mathrm{f}}=\mathrm{Da}\,Y_{\mathrm{o}_\infty}^{1.6}\rho^{1.75}Y_{\mathrm{f}}^{0.15}Y_{\mathrm{o}}^{1.6}\exp\left(E/T\right)$$

is the nondimensional fuel reaction rate, and the corresponding flammability limit is $0.5 \leqslant \phi \leqslant 3.4$, given in Ref. [24].

Equation of state

$$\rho T=1 \tag{8}$$

and the viscosity variation with temperature is taken to be

$$\mu=T^{0.7} \tag{9}$$

Liquid Phase

Continuity

$$\frac{\partial(\rho_1 u_1)}{\partial z}+\frac{1}{r}\frac{\partial(\rho_1 v_1 r)}{\partial r}=0 \tag{10}$$

z Momentum

$$\rho_1 u_1\frac{\partial u_1}{\partial z}+\rho_1 v_1\frac{\partial u_1}{\partial r}=-\frac{\partial P_1}{\partial z}+\frac{\partial}{\partial z}\left\{\frac{\mu_1}{\sqrt{\mathrm{Gr}_1}}\left[2\frac{\partial u_1}{\partial z}-\frac{2}{3}\left(\frac{1}{r}\frac{\partial}{\partial r}(rv_1)+\frac{\partial u_1}{\partial z}\right)\right]\right\}$$

$$+\frac{1}{r}\frac{\partial}{\partial r}\left[\frac{\mu_1}{\sqrt{\mathrm{Gr}_1}}r\left(\frac{\partial u_1}{\partial r}+\frac{\partial v_1}{\partial z}\right)\right] \tag{11}$$

r Momentum

$$\rho_1 u_1 \frac{\partial v_1}{\partial z} + \rho_1 v_1 \frac{\partial v_1}{\partial r} = -\frac{\partial P_1}{\partial r} + \frac{1}{r}\frac{\partial}{\partial r}\left\{ r\frac{\mu_1}{\sqrt{\mathrm{Gr}_1}}\left[2\frac{\partial v_1}{\partial r} - \frac{2}{3}\left(\frac{1}{r}\frac{\partial}{\partial r}(rv_1) + \frac{\partial u_1}{\partial z}\right)\right]\right\} + \frac{\partial}{\partial z}\left[\frac{\mu_1}{\sqrt{\mathrm{Gr}_1}}\left(\frac{\partial u_1}{\partial r} + \frac{\partial v_1}{\partial z}\right)\right] + \frac{\mu_1}{\sqrt{\mathrm{Gr}_1}}\frac{1}{r}\left\{\frac{2v_1}{r} - \frac{2}{3}\left[\frac{1}{r}\frac{\partial}{\partial r}(rv_1) + \frac{\partial u_1}{\partial z}\right]\right\} \tag{12}$$

Gas Phase Boundary Conditions

At $z \to -\infty$ (far upstream),

$$\frac{\partial u}{\partial z} = \frac{\partial v}{\partial z} = 0 \qquad T = T_\infty \qquad Y_f = 0 \qquad Y_o = 1 \tag{13}$$

Note that the ambient oxygen index becomes unity because the mass fraction of the oxidizer ($\bar{Y}_o$) is normalized by its ambient value.

At $z \to +\infty$ (far downstream),

$$\frac{\partial u}{\partial z} = \frac{\partial y}{\partial z} = \frac{\partial T}{\partial z} = \frac{\partial Y_f}{\partial z} = \frac{\partial Y_o}{\partial z} = 0 \tag{14}$$

These conditions imply that there is no downstream influence on the upstream.

At $r \to +\infty$,

$$\frac{\partial u}{\partial z} = \frac{\partial v}{\partial z} = 0 \qquad T = T_\infty \qquad Y_f = 0 \qquad Y_o = 1 \tag{15}$$

Along the symmetric lines at $r = 0$, $z < -0.5$ or $z > 0.5$,

$$\frac{\partial u}{\partial r} = v = \frac{\partial T}{\partial r} = \frac{\partial Y_f}{\partial r} = \frac{\partial Y_o}{\partial r} = 0 \tag{16}$$

Liquid Phase Boundary Conditions

Along the symmetric lines at $r = 0$, $-0.5 < z < 0.5$,

$$\frac{\partial u_1}{\partial r} = v_1 = 0 \tag{17}$$

Gas-Liquid Interface Boundary Conditions

Along the droplet surface, $-0.5 < z < 0.5, \sqrt{z^2 + r^2} = 0.5$,

$$V_t = V_{t1} \qquad G_w = \rho_w V_n = \rho_1 3 V_{n1}$$

$$\mu\left[r\frac{\partial}{\partial r}\left(\frac{V_t}{r}\right) + \frac{1}{r}\frac{\partial(V_n)}{\partial\theta}\right] = \mu_1\left[r\frac{\partial}{\partial r}\left(\frac{V_{t1}}{r}\right) + \frac{1}{r}\frac{\partial(V_{n1})}{\partial\theta}\right]$$

$$G_w Y_{ow} = \left(\frac{\mu}{\sqrt{\mathrm{Gr}}\,\mathrm{Pr}\,\mathrm{Le}}\right)_w \frac{\partial Y_o}{\partial n}\bigg|_w$$

$$G_w Y_{fw} = G_w + \left(\frac{\mu}{\sqrt{\mathrm{Gr}}\,\mathrm{Pr}\,\mathrm{Le}}\right)_w \frac{\partial Y_f}{\partial n}\bigg|_w \tag{18}$$

$$\frac{\partial T}{\partial n}\bigg|_w = \frac{G_w}{\mu_w} L\sqrt{\mathrm{Gr}}\,\mathrm{Pr}$$

$$Y_{fw} = 1\Big/\left[1 + \frac{M_a}{M_f}\left(\frac{\bar{P}_\infty}{\bar{P}_v} - 1\right)\right]$$

where $\bar{P}_v = 60.612\exp(A)$, in which $A = [1/(1-X)][-8.51838X + 0.34163X^{1.5} - 5.73683X^3 + 8.32581X^6]$ and $X = 1 - \bar{T}/513.9$ [26].

The corresponding definitions can be found in the Nomenclature. Since the values of variables cannot be specified along the interface, an iteration procedure is required in order to find the surface temperature, velocity, species mass concentrations, and evaporation rate simultaneously.

Because the flow field configuration shown in Figure 1 is irregular, an r-z body-fitted coordinate system is used to generate grids for gas and liquid phases, in which the grid generation technique developed by Thomas and Middlecoff [27] is adopted. The computational domain can be reduced to the half-domain because of symmetry with respect to the z axis. The grid used for the gas phase is (115, 51), and there are 19 grid points along the half-droplet surface in the angular direction. The liquid-side grid is (25, 15). The computational domain for the gas phase is $z_{min} = -22$, $z_{max} = 30$, and $r_{max} = 30$. By means of the grid generation technique, the computational domain is composed of equally spaced and square grids ($\Delta\eta = \Delta\xi = 1$). Then the transformed governing equations resulting from the mapping process are integrated and discretized in the computational domain. The upwind scheme is adopted for the convection term, and the central difference scheme for the diffusion term. Finally, the SIMPLEC algorithm developed by Van Doormaal and Raithby [28] is used. A detailed development of this numerical scheme and verification of its numerical accuracy are given by Huang and Chen [23] and by Chen and Huang [29], whose convergence criteria, taken as the maximal residual for each control volume, are below 1.0×10^{-4}.

Table 1. Nondimensional parameters

Symbol	Definition	Value
Da	$\bar{B}\bar{d}/\bar{\rho}^*\bar{U}_{ref}$	variable
Gr	$\bar{g}(\bar{\rho}_\infty - \bar{\rho}_f)\bar{d}^3/\bar{\rho}^*\bar{\nu}^{*2}$	variable
Pr	$\bar{\nu}/\bar{\alpha}$	0.811
Le	$\bar{\alpha}/\bar{D}$	1.0
Q	$\bar{Q}/\bar{C}_p\bar{T}^*$	18.21
E	$\bar{E}/R^\circ\bar{T}^*$	12.08
L	$\bar{L}/\bar{C}_p\bar{T}^*$	0.6767

RESULTS AND DISCUSSION

The droplet is ethanol, and Table 1 lists all of the normalized parameters. The corresponding properties and the values used in chemical kinetics are summarized in Table 2. Most of the data are the same as those in Ref. [23], which facilitates comparison. The parametric study is based on changing the droplet diameter to study its influence on the flame and droplet interior structures. From Eq. (1) and Table 1, we see that varying the droplet diameter will directly change U_{ref}, which represents the characteristic velocity of induced convection in a gravitational field. Consequently, both Da and Gr are affected. According to the definitions in Table 1, a decrease in droplet diameter leads to a reduction in both Da and Gr. From the energy equation, Eq. (5), a reduction in Da contributes to a lower heat generation rate. On the other hand, the penetration of forward heat conduction is intensified by a decrease in Gr. These two opposing effects, or two competing mechanisms, complicate the burning behavior of a droplet. In order to compare with the results of our previous study [23], the same environment and droplet diameter computational range, from 1.02 to 0.51 mm, were used.

Six cases of predicted results are selected to illustrate the droplet flame and internal flow characteristics. They are shown together in Figure 2. The flame structures, a combination of isotherm distribution and velocity vector field, are shown on the left-hand side. On the right-hand side, the resultant evaporation velocity ($\sqrt{v_t^2 + v_n^2}$) along the droplet surface and the streamlines within the

Table 2. Properties and chemical kinetics

Item	Symbol	Value	Unit
Density (reference)	$\bar{\rho}^*$	0.2829	kg/m^3
Viscosity (reference)	$\bar{\mu}^*$	4.81×10^{-5}	kg/(m s)
Temperature (reference)	$\bar{T}^*$	1250	K
Specific heat	$\bar{C}_p$	1.186	kJ (kg K)
Frequency factor	$\bar{B}$	9.36×10^7	kg/(m^3 s)
Activation energy	$\bar{E}$	1.25×10^5	kJ (kg mol)
Heat of reaction	$\bar{Q}$	2.70×10^4	kJ (kg fuel)

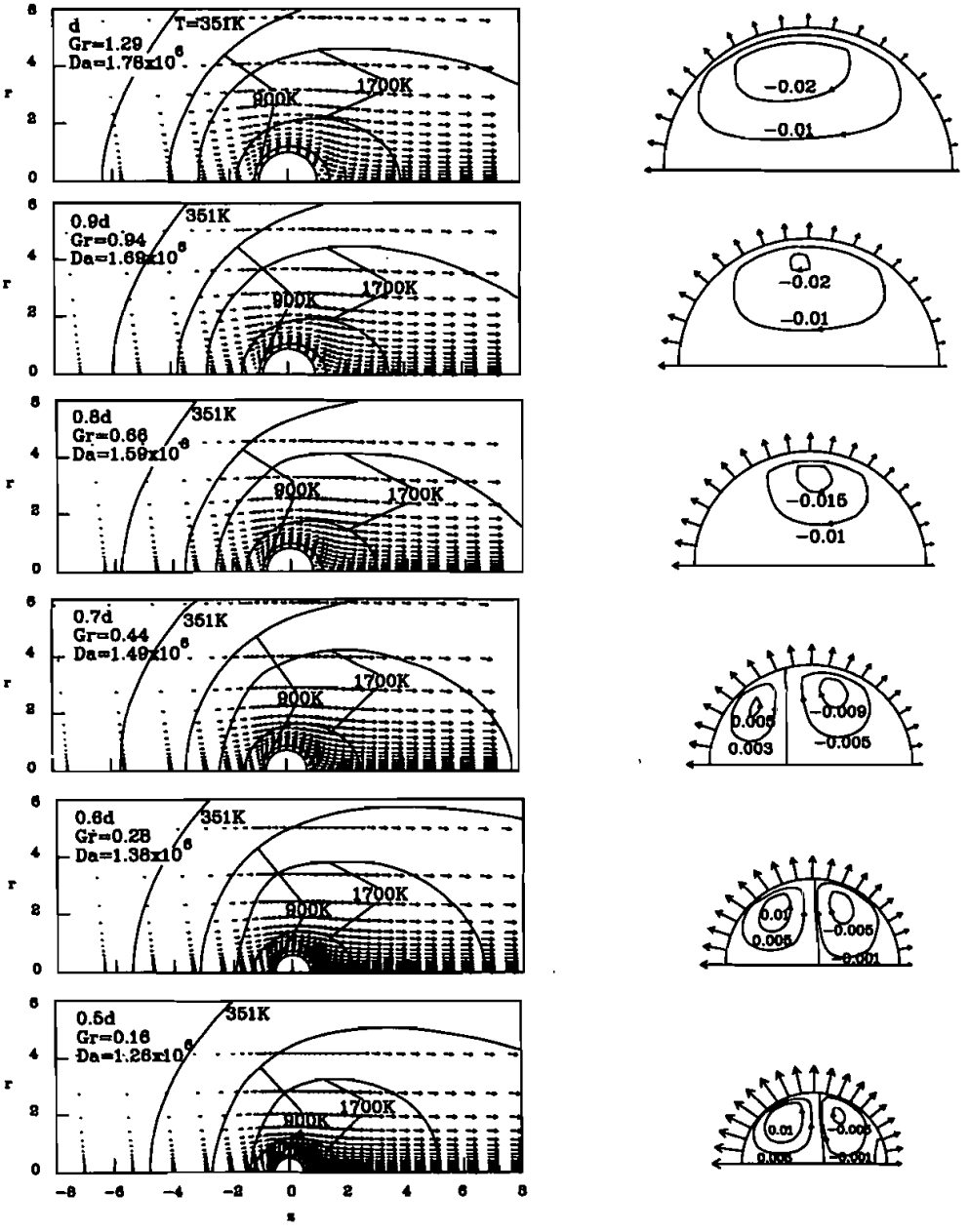

Figure 2. Flame structures.

droplet are shown for each case. The parameters Da and Gr are also listed in each instance. Note that the velocity and length scales are all divided by the references used in the case of $d = 1.02$ mm in order to clearly demonstrate the relative variation during the process of parametric study.

The flame appearance (represented by isotherms) should be spherical in zero gravity (Gr = 0). As shown in Figure 2, the flame always encloses the droplet, i.e., it is an envelope flame, and it appears to be oval in all cases, indicating that it is influenced by gravity. The flame size contracts as droplet diameter shrinks. In the meantime, the isothermal symmetry with respect to $z = 0$ becomes more apparent, indicating that the flame shape tends to be spherical when droplet diameter is small, or when Gr is low, because the induced flow strength becomes weaker. The evaporation velocity in the radial direction increases with a decrease of droplet diameter (see Figure 4*a*), since the flame is closer to the droplet and the heat flux received per unit of surface area increases. The larger blowing velocity causes more excessive reactant leakage and, subsequently, a lower flame temperature. Therefore we can see that the area of the high-temperature region, especially at the front of the droplet, is greatly reduced for small droplets; see the isotherm $T = 1700$ K, for instance.

Jog et al. [17] adopt a thin-flame-sheet approximation, so the flame zone is infinitely thin. The present model uses finite-rate chemical kinetics, which results in a broad reaction (flame) zone. However, both flames have the same tendency, which appears to be asymmetric with respect to $z = 0$ but with varying degrees of asymmetry because they are the direct consequence of forced or free convection.

We can see that flow in the velocity field is insignificant far upstream until it senses high temperature, for instance, $T = 900$ K. A pressure rise occurs in the flame due to local thermal expansion. Ahead of the flame, the flow is still accelerated rather than decelerated because the upward buoyancy force overcomes the adverse pressure gradient. Behind the flame, the buoyancy force is reinforced by the favorable pressure gradient, accelerating the flow substantially. The presence of accelerating fluid flow in the vicinity of the flame was also observed in the experiments of Isoda and Kumagai [5] and Aldred et al. [30]. Far downstream of the droplet, flows for each case tend to become parallel with the symmetric line ($r = 0$). Similar behavior could be seen as well in the work by Jog et al. [17], although the droplet was subjected to forced convection in that study.

It is interesting to see flow in the gas phase around the forward stagnation point area. A reverse flow begins to appear when the droplet diameter is $0.9d_0$. It results from the interaction between the induced flow and the blowing velocity due to evaporation. We can see in Figure 2 that the blowing velocity in the front half of the droplet counteracts the incoming induced flow, which is decelerated when approaching the droplet. As soon as the former is stronger than the latter, a reverse flow occurs. The blowing velocity becomes greater as the droplet diameter is smaller (see Figure 4*a*). Therefore the ratio of the size of reverse flow to its own droplet size grows as the diameter decreases. Since the gas-liquid interface is not stationary, its direction of motion depends on the local shear stress, which is mainly determined by the gas velocity gradient just outside the interface. The distributions of resultant shear stresses are shown in Figure 3, which is discussed below. As just mentioned, it further determines the flow pattern within the droplet, illustrated on the right-hand side of Figure 2.

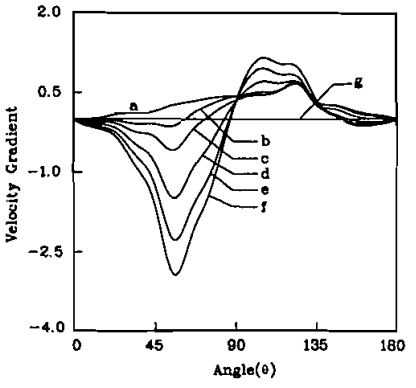

Figure 3. Nondimensional velocity gradient along the droplet surface: tangential velocity gradient, curve a, d_0; curve b, $0.9d_0$; curve c, $0.8d_0$; curve d, $0.7d_0$; curve e, $0.6d_0$; curve f, $0.5d_0$; curve g, radial velocity gradient.

When the droplet diameter is $\geqslant 0.8d_0$, the streamlines in the liquid phase show a clockwise single-vortex cell within the droplet (Figure 2). In Figure 3, although the shear stresses of $d = 0.9d_0$ and $0.8d_0$ for $\theta < 90°$ are negative, they are not strong enough to conquer the inertia of the liquid itself. Therefore the vortex retains the clockwise direction, but its strength declines. Within the droplet, Jog et al. [17] found that the strength of the circulatory vortex decreases with an increase in the radial evaporation velocity. This finding was the same as that we just mentioned. Beyond that diameter, a counterclockwise cell starts tc appear in the neighborhood of the forward stagnation point. Apparently, the reverse shear stress outweighs the inertia completely at this point. The relative size of the reverse cell grows with a decrease in droplet diameter because the magnitude of the shear stress becomes larger. Near the rear stagnation point, the shear stress becomes negative again when $d < 0.8d_0$ (Figure 3). However, once the droplet diameter has shrunk to $0.5d_0$, a third counterclockwise cell begins to appear, for reasons previously stated.

Experimental observation [31] has determined that larger droplets can usually retain a more or less spherical shape while burning, but smaller droplets do not. Our results can explain this behavior. We assume that the droplet always retains its spherical shape, but in actuality, the shape is distorted and the extra reverse cell may not arise. In other words, a small droplet will begin changing shape from the region around the forward stagnation point in a gravitational environment. Reverse shear stress will play an important role in determining droplet shape when droplets burn in low-Gr regimes. Generally speaking, a single cell resembling a Hill's spherical vortex was found by many investigators in an evaporating droplet subjected to high-temperature forced convection. In such cases, the flow strength around the droplet is still greater than the evaporation velocity. However, in the present study the situation is quite different because the induced flow near the burning droplet is slow and the evaporation is enhanced substantially by combustion.

Figure 3 shows the two-component distributions of dimensionless shear stress along the interface, whose location is indicated by the angle θ. As we can see from Eq. (18), the total shear stress along the droplet surface has two components: a tangential velocity gradient due to gas flow, and a radial one due to the blowing velocity. It can be seen in Figure 3 that the component generated by the radial

velocity gradient is almost equal to zero. Therefore we can conclude that the total shear stress is completely dominated by the gas stream near the droplet. This agrees with the conclusions arrived at by Renksizbulut and Haywood [13] when they studied an evaporating droplet subjected to high-temperature forced convection. In their study, the surface velocity gradient, $\partial v_\theta / \partial r$, was always the largest gradient and dominated the surface shear stress. The existence of the extra reverse cell was also reported by Ayyaswamy et al. [16] in a low-Re flow regime. However, the extra reverse cell in that study was attributed to nonuniformity of radial evaporation velocity in the angular direction. The mechanism is quite different from that mentioned previously.

Figures 4*a* and 4*b* show the distributions of radial velocity and tangential velocity along the droplet surface, respectively. In Figure 4*a* the radial velocity increases with a decrease in droplet diameter. The variation of radial velocity in the region $\theta < 90°$ is insignificant when the droplet diameter is smaller and the induced velocity in the gas phase becomes weaker. The radial velocity would be a constant if the induced velocity was zero, a spherical flame. This indicates that the flame shape tends to become spherical in the region $\theta < 90°$. This phenomenon can also be observed in Figure 2.

In Figure 4*b*, when only one cell occurs, $d \geq 0.8d_0$, the tangential velocity is from zero to negative, then to positive, finally reaching zero at the rear stagnation

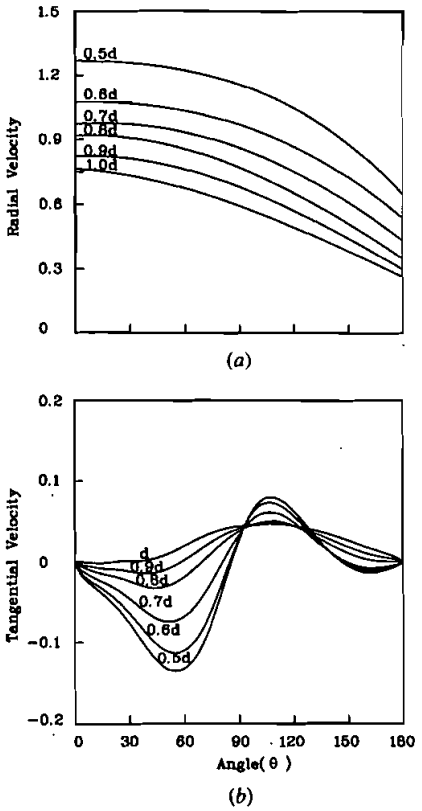

Figure 4. Nondimensional velocity distributions along the droplet surface.

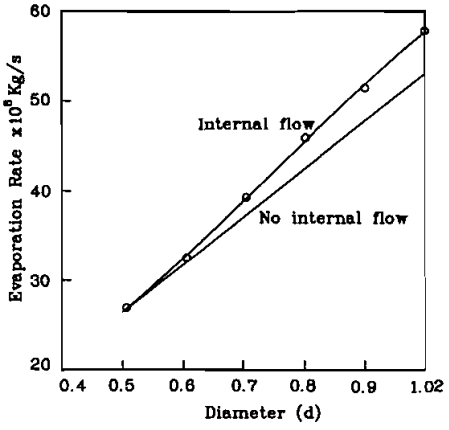

Figure 5. Total mass evaporation rate versus droplet diameter.

point. However, for $d < 0.8d_0$, where another reverse cell shows up, the tangential velocity becomes negative just before it reaches the rear stagnation point.

Figure 5 is the total dimensional evaporation rate as a function of droplet diameter. In order to aid understanding of the effect of considering the internal circulation, the results of using the porous solid sphere assumption in Ref. [23] are also shown in this figure. We can see that the evaporation rate in the present study was greater than that without internal circulation. However, the difference narrows as the droplet diameter shrinks. The evaporation rates for both cases have the same value when the diameter is 0.51 mm. The effect of internal circulation on mass evaporation rate can be ignored if the droplet is very small. In other words, the commonly used porous solid sphere assumption is still useful in considering droplet combustion as long as the droplet size is small enough. However, because of gas-liquid interface motion in larger droplets, the evaporation velocity is no longer normal to the droplet surface (see Figure 2). This moving interface will draw the high-temperature isotherms closer to the droplet surface, which contributes to a higher evaporation rate. Of course, the flame was stronger in the present study. It is known from experimental observation [15] that internal motion within the droplet enhances internal heat transport during droplet heating. The present results, which consider the burning rather than the heating of a single droplet, show that for large droplets the internal circulation will increase the evaporation rate as well.

CONCLUDING REMARKS

The steady combustion characteristics of a single droplet in a gravitational field with variable properties have been studied numerically. The gas phase combustion model includes the full set of conservation equations in r-z coordinates and a one-step overall chemical reaction with finite-rate global kinetics. For the liquid phase, the continuity and momentum conservation equations were used to describe flow motion inside the droplet. At the moving gas-liquid interface, a thermodynamic equilibrium was assumed. The shear stress, tangential velocity, and

temperature are continuous, and the mass flux, energy, and species were conserved at the interface. A grid generation technique and the SIMPLEC algorithm were applied to handle the irregular flow field and solve the problem in an equal-square transform plane.

The parametric study was based on changing droplet diameter. Detailed flame structures, such as the isotherm distribution and the velocity vector field in the gas phase, the flow within the droplet, and the shear stress and velocity distributions along the droplet surface, were illustrated graphically. In the gas phase, a naturally convective flow was present around the droplet. A reverse flow, resulting from the interaction between the induced flow and blowing velocity, was found at the forward part of the droplet when its diameter shrank. The flame was oval in shape, but it tended to become spherical as droplet diameter got very small. The flame size contracted with a decrease in droplet size. One, two, or three cells were present within the burning droplet, depending on its diameter. The two-component distributions of shear stress along the droplet surface are illustrated graphically. Results show that the shear stress due to the tangential velocity gradient determined the flow pattern inside the droplet. Comparing total mass evaporation rate with that in the solid porous sphere assumption model, the present computed results show that internal flow in the droplet can be ignored when the droplet diameter is very small. Otherwise, the internal circulation will increase the evaporation rate for a large droplet.

As to the future extensions of this work, it would be interesting to take droplet heating into consideration; then combustion would certainly become a transient process. This will introduce many difficulties and complexities. The simulation of gas phase ignition is the ultimate goal of our research. Also, similar to Kneer et al. [22], we intend to take into consideration the variable liquid properties as a function of temperature, to further eliminate the difference from the real situation. These issues will be explored in the near future.

REFERENCES

1. A. Williams, Combustion of Droplet of Liquid Fuel: A Review, *Combust. Flame*, vol. 21, pp. 1–31, 1973.
2. G. M. Faeth, Current Status of Droplet and Liquid Combustion, *Prog. Energy Combust. Sci.*, vol. 3, pp. 191–224, 1977.
3. C. K. Law, Recent Advances in Droplet Vaporization and Combustion, *Prog. Energy Combust. Sci.*, vol. 8, pp. 171–201, 1982.
4. S. Kumagai and H. Isoda, Combustion of Fuel Droplets in a Falling Chamber, *Sixth Symp. (Int.) on Combust.*, pp. 726–731, The Combustion Institute, Reinhold, New York, 1957.
5. H. Isoda and S. Kumagai, New Aspects of Droplet Combustion, *Seventh Symp. (Int.) on Combust.*, pp. 523–531, The Combustion Institute, Butterworths, London, 1959.
6. S. Okajima and S. Kumagai, Experimental Studies on Combustion of Fuel Droplets in Flowing Air Under Zero- and High-Gravity Conditions, *Nineteenth Symp. (Int.) on Combust.*, pp. 401–407, The Combustion Institute, Pittsburgh, Pennsylvania, 1982.
7. G. K. Batchelor, On Steady Laminar Flow with Closed Streamlines at Large Reynolds Number, *J. Fluid Mech.*, vol. 1, pp. 177–190, 1956.

8. V. I. Rivkind, G. M. Ryskin, and G. A. Fishbein, Flow Around a Spherical Drop at Intermediate Reynolds Number, *J. Appl. Math. Mech.*, vol. 40, pp. 687–691, 1976.
9. S. Prakash and W. A. Sirignano, Liquid Fuel Droplet Heating with Internal Circulation, *Int. J. Heat Mass Transfer*, vol. 21, pp. 885–895, 1978.
10. S. Prakash and W. A. Sirignano, Theory of Convective Droplet Vaporization with Unsteady Heat Transfer in the Circulating Liquid Phase, *Int. J. Heat Mass Transfer*, vol. 23, pp. 253–268, 1980.
11. L. J. Huang and P. S. Ayyaswamy, Evaporation of a Moving Liquid Droplet: Solution for Intermediate Reynolds Numbers, *Int. Commun. Heat Mass Transfer*, vol. 17, pp. 27–38, 1990.
12. C. H. Chiang, M. S. Raju, and W. A. Sirignano, Numerical Analysis of Convective, Vaporizing Fuel Droplet with Variable Properties, Paper AIAA-89-0834.
13. M. Renksizbulut and R. J. Haywood, Transient Droplet Evaporation with Variable Properties and Internal Circulation at Intermediate Reynolds Numbers, *Int. J. Multiphase Flow*, vol. 14, pp. 189–202, 1988.
14. M. Renksizbulut, R. Nafziger, and R. J. Haywood, A Detailed Examination of Gas and Liquid Phase Transient Processes in Convective Droplet Evaporation, *J. Heat Transfer*, vol. 111, pp. 495–502, 1989.
15. A. C. Lin, Microexplosion and Heating Mechanism of Aluminum/Carbon Slurry Droplets, Ph.D. thesis, National Tsing Hua University, Hsinchu, Taiwan, 1991.
16. P. S. Ayyaswamy, S. S. Sadhal, and L. J. Huang, Effect of Internal Circulation on the Transport to a Moving Drop, *Int. Commun. Heat Mass Transfer*, vol. 17, pp. 689–702, 1990.
17. M. A. Jog, P. S. Ayyaswamy, and I. M. Cohen, Evaporation and Combustion of a Slowly Moving Liquid Fuel Droplet: Higher-Order Theory, *J. Fluid Mech.*, vol. 307, pp. 135–165, 1996.
18. C. K. Law, Unsteady Droplet Combustion with Droplet Heating, *Combust. Flame*, vol. 26, pp. 17–22, 1976.
19. C. K. Law and W. A. Sirignano, Unsteady Droplet Combustion with Droplet Heating—II: Conduction Limit, *Combust. Flame*, vol. 28, pp. 175–186, 1977.
20. H. R. Dwyer and B. R. Sanders, A Detailed Study of Burning Fuel Droplets, *Twenty-First Symp. (Int.) on Combust.*, pp. 633–639, The Combustion Institute, Pittsburgh, Pennsylvania, 1986.
21. H. R. Dwyer and B. R. Sanders, Calculations of Unsteady Reacting Droplet Flows, *Twenty-Second Symp. (Int.) on Combust.*, pp. 1923–1929, The Combustion Institute, Pittsburgh, Pennsylvania, 1988.
22. R. Kneer, M. Schneider, B. Noll, and S. Wittig, Diffusion Controlled Evaporation of a Multicomponent Droplet: Theoretical Studies on the Importance of Variable Liquid Properties, *Int. J. Heat Mass Transfer*, vol. 36, no. 9, pp. 2403–2415, 1993.
23. L. W. Huang and C. H. Chen, Single Droplet Combustion in a Gravitational Environment, *Wärme-und-Stoffübertragung*, vol. 29, pp. 415–423, 1994.
24. C. K. Westbrook and F. L. Dryer, Simplified Reaction Mechanisms for Oxidation of Hydrocarbon Fuels in Flames, *Combust. Sci. Technol.*, vol. 27, pp. 31–43, 1981.
25. C. H. Chen and W. H. Hou, Diffusion Flame Stabilization and Extinction Under Natural Convective Flows, *Combust. Flame*, vol. 83, pp. 309–324, 1991.
26. R. C. Reid, J. M. Prausnitz, and B. E. Poling, *The Properties of Gases and Liquids*, McGraw-Hill, Singapore, 1988.
27. P. D. Thomas and J. H. Middecoff, Direct Control of the Grid Point Distribution in Meshes Generated by Elliptic Equations, *AIAA J.*, vol. 18, pp. 652–656, 1980.
28. J. P. Van Doormaal and G. D. Raithby, Enhancements of the Simple Method for Predicting Incompressible Fluid Flows, *Numer. Heat Transfer*, vol. 7, pp. 147–163, 1984.

29. C. H. Chen and L. W. Huang, Heat Transfer for Fluid Flow Past an Isothermal Heated Sphere, *Chinese Soc. Mech. Eng.*, vol. 14, pp. 200–206, 1993.
30. J. W. Aldred, J. C. Patel, and A. Williams, The Mechanism of Combustion of Droplets and Spheres of Liquid n-Heptane, *Combust. Flame*, vol. 17, pp. 139–148, 1971.
31. S. Kumagai, T. Sakai, and S. Okajima, Combustion of Free Fuel Droplets in a Freely Falling Chamber, *Thirteenth Symp. (Int.) on Combust.*, pp. 779–785, The Combustion Institute, Pittsburgh, Pennsylvania, 1971.